

Microscopic theory of optical nonlinearities and spontaneous emission lifetime in group-III nitride quantum wells

W. Chow

Sandia National Laboratories, Albuquerque, New Mexico 87185-0601

M. Kira

Department of Physics and Material Sciences Center, Philipps-University, Renthof 5, D-35032 Marburg, Germany

S. W. Koch

Sandia National Laboratories, Albuquerque, New Mexico 87185-0601

and Department of Physics and Material Sciences Center, Philipps-University, Renthof 5, D-35032 Marburg, Germany

(Received 5 January 1999; revised manuscript received 3 March 1999)

Microscopic calculations of the absorption and luminescence spectra are presented for wide bandgap $\text{Ga}_{1-x}\text{In}_x\text{N}/\text{GaN}$ quantum well systems. Whereas structures with narrow well widths exhibit the usual excitation-dependent bleaching of the exciton resonance without shifting spectral position, a significant blueshift of the exciton peak is obtained for wider quantum wells. This blueshift, which is also present in the excitation-dependent luminescence spectra, is attributed to the interplay between the screening of a strain induced piezoelectric field and the density dependence of many-body Coulomb effects. The calculations also show an over two orders of magnitude increase in the spontaneous electron-hole-pair lifetime with well width, due to the reduction of the electron-hole wave function overlap in the wider wells. The resulting decrease in spontaneous emission loss is predicted to lead to improved threshold properties in wide quantum well lasers. [S0163-1829(99)00727-4]

I. INTRODUCTION

The physical properties of wide bandgap group-III quantum-well systems are currently under intense investigation, mostly because of their substantial application potential as light emitters and semiconductor lasers in the ultraviolet to blue-green wavelength region.¹ Additionally, these materials exhibit interesting excitation dependent nonlinear behavior due to the intricate interplay between the strong attractive electron-hole Coulomb interaction, which lead to significant excitonic signatures in the optical spectra, and the quantum-confined Stark effect caused by piezoelectric fields. Such fields are present, for example, in wurtzite $\text{Ga}_{1-x}\text{In}_x\text{N}/\text{GaN}$ systems because of the strain induced lattice mismatch.² The relative magnitude of excitonic and piezoelectric effects depends sensitively on quantum-well width and plasma density, because of many-body interactions leading to effects including screening, dephasing, bandgap renormalization, and phase-space filling.^{3,4}

In this paper, we present a theoretical investigation of the intricate interplay of the different nonlinear effects and study their influence on the absorption and luminescence spectra, as well as intrinsic spontaneous carrier lifetime. For this purpose, we use a previously developed microscopic theory for the excitation-dependent optical response.⁴ This theory is based on the semiconductor Bloch equations,³ where the damping and dephasing processes are treated at the level of quantum kinetic theory. Such an approach has several advantages over the more familiar calculations based on the relaxation rate approximation.⁵⁻⁷ It eliminates the dephasing rate as a free parameter, and therefore gives more precise predic-

tions of optical properties. Equally important, it includes an important piece of physics involving contributions from non-diagonal Coulomb correlations. These contributions, which are unique to semiconductor systems and neglected in relaxation rate treatments, are found to be important in describing the experimental shape and carrier density dependence of absorption and gain spectra in conventional III-V lasers.⁸

The theoretical approach is described in Sec. II, where we show the adaptation of the general theory to the treatment of our particular problem. Basically, some simplifications are possible because our investigation is limited to the linear optical response to a probe beam in the presence of an electron-hole plasma. On the other hand, the details of the multiband bandstructure has to be included, because we are comparing different quantum well structures. Also discussed in this section is the treatment of the quantum-confined Stark effect in the bandstructure calculations. Section III presents absorption and spontaneous emission spectra that are calculated with the theory described in Sec. II. By comparing the absorption and emission spectra for two InGaN/GaN quantum well structures of very different well widths, we show the interplay of bandstructure and Coulomb effects. In particular, we see in wide quantum well structures, where the quantum-confined Stark effect is appreciable, an absence of the usual strong cancellation of competing many-body effects that is responsible for the carrier density independence of the excitonic peak position during the bleaching of the resonance. Because shifts in the exciton resonance with excitation are very rare,⁹ examples of exceptions are always interesting and noteworthy. The same interplay of bandstruc-

ture and Coulomb effects also leads to significant variation in oscillator strength with carrier density and quantum well configuration. One result is a strong dependence of the spontaneous emission lifetime with quantum well width, which we discuss in Sec. IV. The calculations show that as much as two orders of magnitude difference in the spontaneous electron-hole-pair lifetime is possible with quantum well width ranging from 2 to 4 nm. The implications of the reduction in oscillator strength to laser behavior are also discussed. Finally, we summarize our results in Sec. V.

II. THEORETICAL APPROACH

From Maxwell's equations, the linear absorption experienced by a plane wave optical field is (in MKS units) (Ref. 3)

$$\alpha(\omega) = \frac{\omega}{\varepsilon_0 n c E} \text{Im} P, \quad (1)$$

where E and ω are the electric field amplitude and frequency of the optical wave, ε_0 and c are the permittivity and speed of light, respectively, in vacuum, and n is the background refractive index. According to semiclassical laser theory, the amplitude P of the polarization induced in the active medium by the optical field is given by³

$$P = \frac{2}{V} \sum_{\nu_e, \nu_h, \vec{k}} (\mu_{\vec{k}}^{\nu_e \nu_h})^* p_{\vec{k}}^{\nu_e \nu_h} e^{i\omega t}, \quad (2)$$

where V is the active region volume, \vec{k} is the transverse (in the quantum well plane) carrier momentum, ν_e (ν_h) identifies the conduction (valence) quantum well subband, $\mu_{\vec{k}}^{\nu_e \nu_h}$ is the optical dipole matrix element, and $p_{\vec{k}}^{\nu_e \nu_h}$ is the microscopic dipole due to an electron-hole pair with electron (hole) momentum \vec{k} ($-\vec{k}$) and subband label ν_e (ν_h). To calculate the microscopic dipoles quantum mechanically, we use a theory for the excitation-dependent optical response.⁴ This theory gives a set of coupled equations of motion for the microscopic polarization, as well as the electron and hole populations $n_{\vec{k}}^{\nu_e}$ and $n_{\vec{k}}^{\nu_h}$, respectively. For the linear optical response, we assume that $dn_{\vec{k}}^{\nu_e}/dt \approx 0$ and $dn_{\vec{k}}^{\nu_h}/dt \approx 0$, so that we have to consider only the polarization equation⁸

$$\begin{aligned} \frac{d}{dt} p_{\vec{k}}^{\nu_e \nu_h} &= -i\omega_{\vec{k}}^{\nu_e \nu_h} p_{\vec{k}}^{\nu_e \nu_h} - i\Omega_{\vec{k}}^{\nu_e \nu_h} (n_{\vec{k}}^{\nu_e} + n_{\vec{k}}^{\nu_h} - 1) \\ &\quad - (\Gamma_{\vec{k}}^{\nu_e} + \Gamma_{\vec{k}}^{\nu_h}) p_{\vec{k}}^{\nu_e \nu_h} + \sum_q (\Gamma_{\vec{k}q}^{\nu_e} + \Gamma_{\vec{k}q}^{\nu_h}) p_{\vec{k}+q}^{\nu_e \nu_h}. \end{aligned} \quad (3)$$

In Eq. (3), the first line describes the oscillation of the polarization at the transition frequency, and the stimulated emission or absorption processes. The transition frequency $\omega_{\vec{k}}^{\nu_e \nu_h}$ and the Rabi frequency $\Omega_{\vec{k}}^{\nu_e \nu_h}$ are given by

$$\omega_{\vec{k}}^{\nu_e \nu_h} = \frac{1}{\hbar} \left(\varepsilon_{e\vec{k}}^{\nu_e} + \varepsilon_{h\vec{k}}^{\nu_h} + \varepsilon_{g0} + \sum_{\alpha=e,h} \sum_q V_q^{\nu_e \nu_h \alpha} n_{\vec{k}+q}^{\nu_e \nu_h} \right) \quad (4)$$

and

$$\Omega_{\vec{k}}^{\nu_e \nu_h} = \frac{1}{\hbar} \left(\mu_{\vec{k}}^{\nu_e \nu_h} E e^{-i\omega t} + \sum_q V_q^{\nu_e \nu_h \nu_h \nu_e} p_{\vec{k}+q}^{\nu_e \nu_h} \right), \quad (5)$$

where \hbar is Planck's constant divided by 2π , $\varepsilon_{e(h)\vec{k}}^{\nu_e(\nu_h)}$ is the sum of the electron (hole) confinement and kinetic energies, and ε_{g0} is the unexcited strained bulk material bandgap energy. The many-body modifications in Eqs. (4) and (5) (exchange shift and Coulomb field renormalization, respectively) are described by the terms containing the bare (unscreened) Coulomb potential energy,

$$V_q^{\nu_e \nu_h \nu_h \nu_e} = f_q^{\nu_e \nu_h \nu_h \nu_e} \frac{e^2}{2\varepsilon_b A q}. \quad (6)$$

In the expression for the Coulomb potential energy, ε_b is the permittivity of the host medium, e is the electron charge, and A is the area of the quantum well layer. The form factor

$$\begin{aligned} f_q^{\nu_e \nu_h \nu_h \nu_e} &= \int_{-\infty}^{\infty} dz \int_{-\infty}^{\infty} dz' u_{\nu_e}(z) u_{\nu_h}(z') \\ &\quad \times e^{-q|z-z'|} u_{\nu_h}(z') u_{\nu_e}(z) \end{aligned} \quad (7)$$

accounts for the effects of the finite quantum well thickness and confinement potential, where $u_{\nu}(z)$ is the envelope part of the quantum well eigenfunctions.

Carrier-carrier correlations, which lead to screening and dephasing, give rise to the second line in Eq. (3). These contributions are treated at the level of quantum kinetic theory in the Markovian limit. They consist of diagonal ($p_{\vec{k}}^{\nu_e \nu_h}$ term) and nondiagonal ($p_{\vec{k}+q}^{\nu_e \nu_h}$ term) contributions. For the diagonal contribution

$$\begin{aligned} \Gamma_{\vec{k}}^{\nu_e \nu_h} &= \frac{2\pi}{\hbar} \sum_{\beta=e,h} \sum_{\nu_\beta} \sum_{q,k'} \left(|W_q^{\nu_e \nu_h \nu_\beta \nu_\beta}|^2 \right. \\ &\quad \left. - \frac{1}{2} \delta_{\nu_e, \nu_\beta} W_q^{\nu_e \nu_h \nu_\beta \nu_\beta} W_{|\vec{k}+q-\vec{k}'|}^{\nu_e \nu_h \nu_\beta \nu_\beta} \right) \\ &\quad \times D(\varepsilon_{\vec{k}}^{\nu_e} + \varepsilon_{\vec{k}'}^{\nu_\beta} - \varepsilon_{\vec{k}+q}^{\nu_e} - \varepsilon_{\vec{k}'-q}^{\nu_\beta}) \\ &\quad \times [n_{\vec{k}+q}^{\nu_e} (1 - n_{\vec{k}'}^{\nu_\beta}) n_{\vec{k}'-q}^{\nu_\beta} + (1 - n_{\vec{k}+q}^{\nu_e}) n_{\vec{k}'}^{\nu_\beta} (1 - n_{\vec{k}'-q}^{\nu_\beta})], \end{aligned} \quad (8)$$

where $D(\Delta) = \delta(\Delta) + i\pi^{-1}\mathcal{P}(\Delta)$, and \mathcal{P} denotes the principal value. We have replaced the bare Coulomb potential energy with the screened one

$$W_q^{\nu_e \nu_h \nu_\beta \nu_\beta} = \frac{V_q^{\nu_e \nu_h \nu_\beta \nu_\beta}}{\varepsilon_q(N)} \quad (9)$$

to account for screening effects from the higher order correlations that are neglected in the derivation of Eq. (3). For the dielectric function $\varepsilon_q(N)$, we use the static Lindhard formula

$$\varepsilon_q(N) = 1 - \sum_{\rho=e,h} \sum_{\nu_\rho} \sum_k V_q^{\nu_\rho \nu_\rho \nu_\rho \nu_\rho} \frac{n_{k-q}^{\nu_\rho} - n_k^{\nu_\rho}}{\varepsilon_{k-q}^{\nu_\rho} - \varepsilon_k^{\nu_\rho}}. \quad (10)$$

There is also a nondiagonal contribution in Eq. (3) that couples polarizations of different \vec{k} 's. The coefficients for the nondiagonal terms are

$$\begin{aligned} \Gamma_{kq}^{\nu_\alpha} = & \frac{2\pi}{\hbar} \sum_{\beta=e,h} \sum_{\nu_\beta} \sum_{k'} \left(|W_q^{\nu_\alpha \nu_\beta \nu_\beta \nu_\alpha}|^2 \right. \\ & \left. - \frac{1}{2} \delta_{\nu_\alpha, \nu_\beta} W_q^{\nu_\alpha \nu_\beta \nu_\beta \nu_\alpha} W_{|k+q-k'|}^{\nu_\alpha \nu_\beta \nu_\beta \nu_\alpha} \right) \\ & \times D(\varepsilon_{k+q}^{\nu_\alpha} + \varepsilon_{k'-q}^{\nu_\beta} - \varepsilon_k^{\nu_\alpha} - \varepsilon_{k'}^{\nu_\beta}) \\ & \times [(1 - n_k^{\nu_\alpha})(1 - n_{k'}^{\nu_\beta})n_{k'-q}^{\nu_\beta} + n_k^{\nu_\alpha}n_{k'}^{\nu_\beta}(1 - n_{k'-q}^{\nu_\beta})]. \end{aligned} \quad (11)$$

The numerical solution of Eq. (3) requires as input the bandstructure properties, specifically, the electron and hole dispersions $\varepsilon_{ek}^{\nu_e}$ and $\varepsilon_{hk}^{\nu_h}$, as well as the dipole matrix elements $\mu_k^{\nu_e \nu_h}$. In this paper, the quantum well bandstructure calculation is performed using $\vec{k} \cdot \vec{p}$ theory and the envelope approximation.¹⁰ In a typical InGaN/AlGaIn quantum well structure, there is a strain-induced electric field E_p in the quantum well. This piezoelectric field, which is perpendicular to the quantum well plane (i.e., in the z direction) may be appreciable because of the large piezoelectric constant d_{31} in wurtzite structures.² To account for its effects, we modify the treatment in Ref. 10 by including an off-diagonal contribution to the electron and hole Hamiltonian

$$H_{\nu_\alpha \nu'_\alpha}^{\text{piezo}} = eE_p(N) \int_{-\infty}^{\infty} dz u_{\nu_\alpha}(z) z u_{\nu'_\alpha}(z), \quad (12)$$

where ν_α and ν'_α are the subbands coupled by the Stark effect, and $u_{\nu_\alpha}(z)$ and $u_{\nu'_\alpha}(z)$ are the corresponding subband envelope functions. The two-dimensional carrier density N dependence in the piezoelectric field comes from the screening caused by the resulting spatial separation in the electron and hole distributions. The net electric field is

$$E_p(N) = E_p(0) + E_{\text{scr}}(N), \quad (13)$$

where

$$E_p(0) = \frac{2d_{31}e}{\varepsilon_b} \left(C_{11} + C_{12} - \frac{2C_{13}^2}{C_{33}} \right) \quad (14)$$

is the piezoelectric field in the absence of carriers and C_{11} , C_{12} , C_{13} , and C_{33} are the elastic constants. We estimate the effective screening field by spatially averaging over the quantum well, the electric field due to the combined electron and hole distributions:

TABLE I. Material parameters for bulk $\text{In}_{0.2}\text{Ga}_{0.8}\text{N}$ used in quantum well bandstructure calculations.

$m_{e,z}/m_0$	0.166	A_1	-7.15
$m_{e,\perp}/m_0$	0.182	A_2	-0.53
		A_5	-3.37
ε_{g0} (eV)	2.967	Δ_1 (eV)	0.020
		Δ_2 (eV)	0.004
μ_{bulk} (nm)	0.241	n	2.27
		$\varepsilon_b/\varepsilon_0$	10.38
a (Å)	3.219	strain	-0.0214
c (Å)	5.247	$d_{13}(10^{-12} \text{ m V}^{-1})$	-1.58
C_{11} (GPa)	371	$(a_{cz}-D_1)$ (eV)	-5.70
C_{12} (GPa)	140	$(a_{c\perp}-D_2)$ (eV)	-9.03
C_{13} (GPa)	101	D_3 (eV)	5.59
C_{33} (GPa)	369	D_4 (eV)	-2.79

$$\begin{aligned} E_{\text{scr}}(N) = & \frac{1}{d} \int_{-d/2}^{d/2} dz_0 \frac{eN}{2\varepsilon_b} \\ & \times \int_{-\infty}^{\infty} dz [|u_e(z)|^2 - |u_h(z)|^2] \frac{z-z_0}{|z-z_0|}, \end{aligned} \quad (15)$$

where d is the quantum well width. We use for the spatial carrier distributions $u_e(z)$ and $u_h(z)$, the lowest order electron and hole subband envelope functions at zone center. The screening field $E_{\text{scr}}(N)$ is determined by iterating Eq. (13) and the solution to bandstructure calculation until convergence is reached.¹¹

The input to the quantum well bandstructure calculation are the bulk material properties such as the effective masses for the electron and holes parallel and perpendicular to the c axis. The hole effective masses may be expressed in terms of the parameters A_1 , A_2 , and A_5 .^{10,12} The energy separation between the hole states at $k=0$ are described by the two energy splittings Δ_1 and Δ_2 . In addition to the elastic constants, the parameters relating to strain effects are the lattice constants a (in to quantum well plane) and c (perpendicular to quantum well plane), the conduction band deformation potentials a_{cz} and $a_{c\perp}$, and the valence band deformation potentials D_1 , D_2 , D_3 , and D_4 . The remaining parameters are the bulk material dipole matrix element μ_{bulk} , the background refractive index n , and the permittivity of the host material ε_b . The values for the above bulk wurtzite material parameters for GaN, InN, and AlN are given in Ref. 13. For $\text{In}_{0.2}\text{Ga}_{0.8}\text{N}$ considered in this paper, we use the weighted averages listed in Table I.

To calculate spontaneous emission spectra, we make use of an often employed experimental method for obtaining absorption and gain spectra. This method uses a relationship derived from detailed balance arguments to deduce absorption spectra from spontaneous emission measurements.¹⁴ For our purpose, we reverse the process and use the same detailed balance relationship

$$S(\omega) = -\frac{1}{\hbar} \left(\frac{n\omega}{\pi c} \right)^2 \alpha(\omega) \left[\exp\left(\frac{\hbar\omega - \mu_{eh}}{k_B T} \right) - 1 \right]^{-1}, \quad (16)$$

to determine the spontaneous emission spectrum $S(\omega)$ from the absorption spectrum $\alpha(\omega)$ calculated using Eq. (1). In

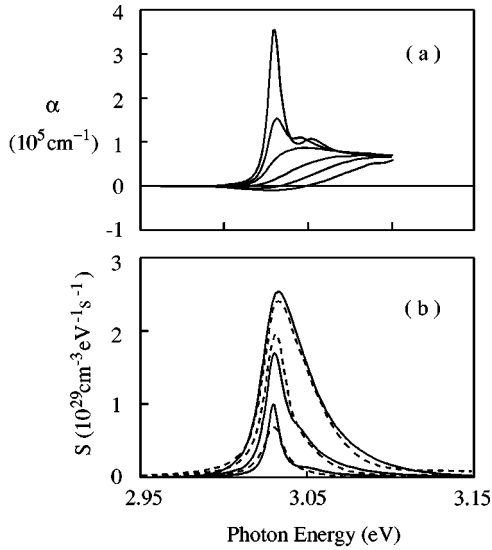


FIG. 1. Calculated (a) TE absorption for 2 nm $\text{In}_{0.2}\text{Ga}_{0.8}\text{N}/\text{GaN}$ quantum well at $T=300$ K, and carrier densities $N=10^{12}$ cm^{-2} to 6×10^{12} in 10^{12} cm^{-2} increments. (b) shows the spontaneous emission spectra for the densities 1, 2, and 3×10^{12} cm^{-2} . The solid lines are obtained from the absorption spectra, and the dashed lines are obtained from the semiconductor luminescence equations (Ref. 15). The material parameters are taken from Table I.

the above equation, k_B is the Boltzmann constant, T is the temperature, and μ_{eh} is electron-hole quasichemical potential energy separation. Such an approach is, of course, not rigorous. However, it does circumvent the complexities associated with quantizing the electromagnetic field. This allows the inclusion into the numerical calculation, the details of the multiband quantum well bandstructure, which are important to our investigation of the intricate interplay of the different nonlinear effects in different quantum well structures. To show the accuracy of this phenomenological approach, we will present in the next section comparisons of its results with those using the fully quantized semiconductor quantum luminescence theory developed recently by Kira *et al.*¹⁵

III. ABSORPTION AND EMISSION SPECTRA

To illustrate the interplay of the bandstructure and many-body effects, we consider a 2 nm and a 4 nm $\text{Ga}_{0.2}\text{In}_{0.8}\text{N}/\text{GaN}$ quantum well structure. Numerically solving the microscopic polarization equations (3), for the steady state solutions yields the absorption spectra shown in Figs. 1(a) and 2(a). For the narrow quantum well [Fig. 1(a)], we see that the low density exciton resonance is gradually bleached with increasing carrier density. At high densities, optical gain (i.e., negative absorption) develops in the spectral vicinity of the original exciton resonance. As is usual in intrinsic quantum well systems, there is negligible shift of the excitonic peak spectral position during the plasma bleaching process. This excitation independent exciton energy is a consequence of the strong cancellation between the weakening of the exciton binding energy and the reduction of the bandgap energy, i.e., between the nondiagonal (field

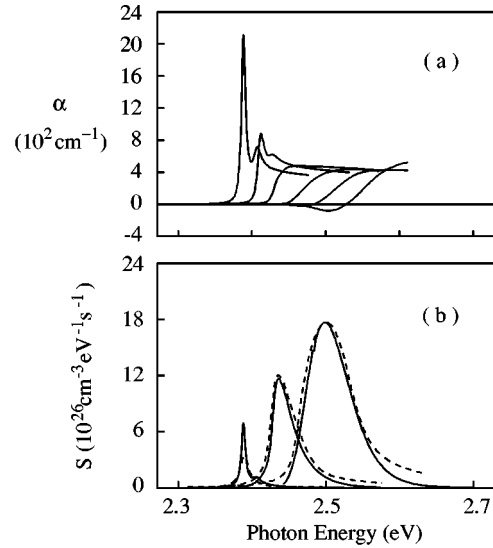


FIG. 2. Same as Fig. 1, but for a 4 nm structure. The densities in (b) are 1, 3, and 5×10^{12} cm^{-2} .

renormalization) and diagonal (self-energy) contributions in the microscopic polarization equations.^{3,4}

As shown in Fig. 2(a), the situation is quite different in the 4 nm $\text{Ga}_{0.2}\text{In}_{0.8}\text{N}/\text{GaN}$ quantum well structure. Because of the weaker quantum confinement in this relatively wide quantum well, the piezoelectric field is able to significantly reduce the overlap between the quantum confined electron and hole wave functions. Consequently, the interband dipole matrix element or oscillator strength is substantially smaller than is the case for the narrow 2 nm quantum well. This intrinsic quantum confined Stark effect (QCSE) also significantly redshifts the exciton absorption peak relative to the flat band situation. As the plasma density increases, the screening of the QCSE increases the electron-hole wave function overlap, and hence, the exciton oscillator strength. Simultaneously, there is a weakening of the piezoelectric field induced redshift, leading to the net blueshift in the exciton resonance and absorption edge with increasing plasma density, as shown in Fig. 2(a). These piezoelectric field related nonlinearities occur in addition to the usual many-body nonlinearities. Due to the stronger piezoelectric field effects in the 4 nm quantum well, the compensation between self-energy and field renormalization contributions to the microscopic interband polarization is perturbed, resulting in the excitation-dependent blueshifting of the exciton resonance and absorption edge. A similar blueshift, also resulting from a perturbation of the abovementioned compensation effects by a real space charge separation, was observed and microscopically analyzed for type-II quantum wells.⁹ Figure 2(a) also shows that the interband absorption, i.e., that part of the spectra well above the absorption edge, increases with increasing excitation density. This again reflects the increasing electron-hole wave function overlap resulting from the gradual screening of the intrinsic QCSE.

Using the absorption spectra in Figs. 1(a) and 2(a), and applying a phenomenological relationship between stimulated and spontaneous emission Eq. (16), we obtain the spontaneous emission spectra shown by the solid curves in Figs. 1(b) and 2(b). These spectra show the increasing spontane-

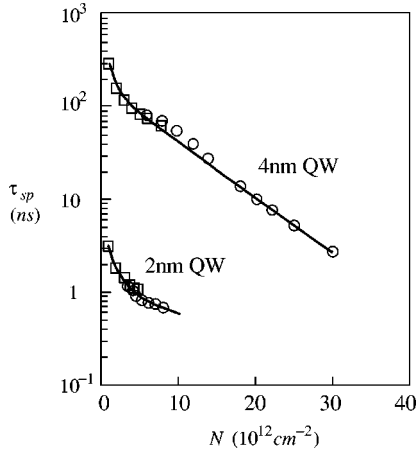


FIG. 3. Radiative lifetime versus carrier density for 2 nm and 4 nm $\text{In}_{0.2}\text{Ga}_{0.8}\text{N}/\text{GaN}$ quantum well at $T=300$ K. The circles are computed from the absorption spectra of Figs. 1 and 2, and the squares are obtained directly from the semiconductor luminescence equations.

ous emission with increasing plasma density. Whereas an excitation-independent peak energy of the luminescence is obtained for the narrow quantum well system, the wide quantum well luminescence exhibits the excitation-dependent blueshift, whose origin is as discussed for the absorption spectra.

To show the accuracy of using Eq. (16), we plotted the results (dashed curves) using the semiconductor quantum luminescence theory.¹⁵ Due to its numerical complexity, this theory can currently only be evaluated for a two-band effective mass model, and using effective dephasing rates extracted from the semiclassical quantum kinetic calculations. The former limits the comparison to low plasma densities, where multiband as well as bandmixing effects are negligible. Comparison of the solid and dashed curves shows that for low densities, where strong excitonic resonances are present in the optical spectra, we obtain deviations between the quantum theory results and the phenomenological conversion. As discussed in Ref. 15 these differences are expected. For increasing densities the agreement improves considerably, being almost quantitative for elevated densities where optical gain is present.

IV. SPONTANEOUS EMISSION LIFETIME

The ordinates of Figs. 1 and 2 show absorption and spontaneous emission amplitudes that differ considerably between wide and narrow quantum wells. This difference should appear in the radiative carrier lifetime, which is a useful quantity to calculate because it is often measured in experiments. Integrating the luminescence spectra in Figs. 1(b) and 2(b) gives the spontaneous emission rate $w_{\text{sp}} = \int_0^\infty d\omega s e(\omega)$, which is the inverse of the radiative carrier lifetime τ_{sp} . The circles in Fig. 3 show the results from the luminescence spectra obtained via the phenomenological conversion approach. At low carrier densities where the two-band effective mass model is valid, the carrier lifetime can also be obtained from the quantum luminescence theory by directly computing the total radiative decay rate of electron-

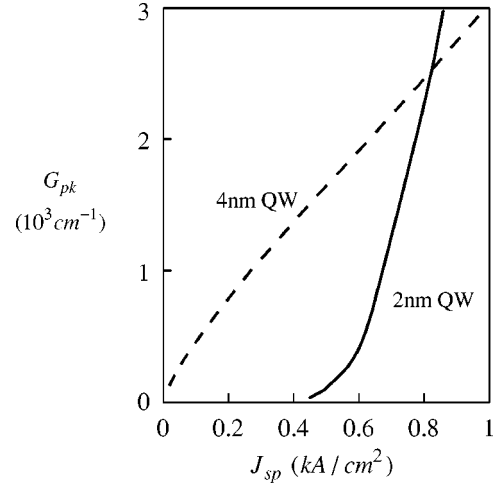


FIG. 4. Peak gain vs spontaneous emission current density for 2 nm and 4 nm $\text{In}_{0.2}\text{Ga}_{0.8}\text{N}/\text{GaN}$ quantum well at $T=300$ K.

hole pairs. The results are shown by the squares, which confirm that both approaches yield close to identical results. These results show that while the narrow 2 nm well has lifetimes typical of conventional III-V materials, the wide 4 nm quantum well shows radiative lifetimes at low plasma densities and room temperature that are two orders of magnitude larger. Similar trends have been observed experimentally for the GaN/AlGaIn system at low temperature.¹⁶ This long lifetime is a direct consequence of the electron-hole wave function separation which is substantial in the wide quantum wells. The figure also shows the carrier density dependence of the radiative lifetime. Here the lifetime decreases with increasing plasma density, due to increased screening of the quantum confined Stark effect and to increased carrier-carrier collisions.

The well width and excitation-dependent oscillator strength due to the quantum confined Stark effect have important implications to group-III nitride lasers. On the one hand, the QCSE reduces the gain in the wide quantum wells. On the other hand, it also reduces their spontaneous emission losses. Figure 4 shows the peak gain (or peak negative absorption) versus spontaneous emission contribution to the current density, for the 2 nm and 4 nm quantum wells. The spontaneous emission current is given by $J_{\text{sp}} = edw_{\text{sp}}$, where e is the electron charge and d is the quantum well width. These curves give the theoretical limit to the threshold current density for a given threshold gain $G_{\text{th}} = G_{\text{pk}}$. From the figure, we see that the reduction in spontaneous emission loss more than compensates the gain reduction in the wide quantum well, so that for typical threshold gains of $G_{\text{th}} = 10^2 - 10^3 \text{ cm}^{-1}$, J_{sp} for the wide well is far lower than that for the narrower well system. Hence, the reduced electron-hole dipole matrix element in the wide $\text{Ga}_{0.2}\text{In}_{0.8}\text{N}/\text{GaN}$ quantum well systems actually benefits laser operation. Comparison of the two curves close to transparency illustrates the very different physical mechanisms leading to the onset of gain. In the 2 nm quantum well, the onset of gain is due to band filling. In contrast, a significant population inversion already exists in the 4 nm quantum well at the onset of gain. Here, the appearance of gain is due to the switch on of the interband dipole matrix element by the screening of QCSE. We wish to emphasize that in an experiment, gain in

the 4 nm quantum well will not occur as close to the origin as shown in Fig. 4, because of the presence of nonradiative losses.

V. CONCLUSION

In summary, the microscopic calculations of the optical absorption and luminescence properties of wide bandgap $\text{Ga}_{0.2}\text{In}_{0.8}\text{N}/\text{GaN}$ quantum well systems predict interesting well-width-dependent nonlinearities. A blueshift with increasing plasma density in absorption and luminescence in relatively wide wells occurs as a consequence of the screening of the piezoelectric field induced quantum confined Stark effect. The quantum confined Stark effect also results in car-

rier lifetimes in the wide wells that are significantly longer than in typical III-V semiconductors. This effect reduces spontaneous emission loss in wide quantum well structures, and can benefit laser threshold properties.

ACKNOWLEDGMENTS

This work was supported in part by the U.S. Department of Energy under Contract No. DE-AC04-94AL85000, by the Deutsche Forschungsgemeinschaft, and by the European Commission. M.K. and S.W.K. thank ACMS, the University of Arizona, and Sandia National Labs for hospitality during the time this work was completed.

-
- ¹S. Nakamura and G. Fasol, *The Blue Laser Diode* (Springer, Berlin, 1997).
- ²A. Bykhovshi, B. Gelmonst, and M. Shur, *J. Appl. Phys.* **74**, 6734 (1993).
- ³For text book discussions, see H. Haug and S.W. Koch, *Quantum Theory of the Optical and Electronic Properties of Semiconductors*, 3rd ed. (World Scientific, Singapore, 1994); W. W. Chow and S. W. Koch, *Semiconductor-Laser Fundamentals: Physics of the Gain Materials* (Springer, Berlin, 1999).
- ⁴F. Jahnke, M. Kira, S. W. Koch, G. Khitrova, E. K. Lindmark, T. R. Nelson, D. V. Wick, J. D. Berger, O. Lyngnes, and H. M. Gibbs, *Phys. Rev. Lett.* **77**, 5257 (1996); F. Jahnke, M. Kira, and S. W. Koch, *Z. Phys. B* **104**, 559 (1997).
- ⁵W. W. Chow, A. F. Wright, and J. S. Nelson, *Appl. Phys. Lett.* **68**, 296 (1996).
- ⁶S.-H. Park and D. Ahn, *Appl. Phys. Lett.* **71**, 398 (1997).
- ⁷S. H. Park and S. L. Chuang, *Appl. Phys. Lett.* **72**, 287 (1998).
- ⁸W. W. Chow, P. M. Smowton, P. Blood, A. Girndt, F. Jahnke, and S. W. Koch, *Appl. Phys. Lett.* **71**, 157 (1995); W. W. Chow, A. F. Wright, A. Girndt, F. Jahnke, and S. W. Koch, *ibid.* **71**, 2608 (1997); A. Girndt, S. W. Koch, and W. W. Chow, *Appl. Phys. A: Mater. Sci. Process.* **66**, 1 (1998).
- ⁹G. Olbright, W. S. Fu, A. Owyong, J. F. Klem, R. Binder, I. Galbraith, and S. W. Koch, *Phys. Rev. Lett.* **66**, 1358 (1991).
- ¹⁰S. L. Chuang and C. S. Chang, *Phys. Rev. B* **54**, 2491 (1996).
- ¹¹J. Wang, J. B. Jeon, M. Sirenko, and K. W. Kim, *IEEE Photonics Technol. Lett.* **9**, 728 (1997).
- ¹²M. Suzuki, T. Uenoyama, and A. Yanase, *Phys. Rev. B* **52**, 8132 (1995).
- ¹³W. W. Chow, M. H. Crawford, A. Girndt, and S. W. Koch, *IEEE J. Sel. Top. Quantum Electron.* **4**, 514 (1998).
- ¹⁴C. H. Henry, R. A. Logan, and F. R. Merritt, *J. Appl. Phys.* **51**, 3042 (1980).
- ¹⁵M. Kira, M. Kira, F. Jahnke, S. W. Koch, J. D. Berger, D. V. Wick, T. R. Nelson, G. Khitrova, and H. M. Gibbs, *Phys. Rev. Lett.* **79**, 5170 (1997); M. Kira, F. Jahnke, and S. W. Koch, *ibid.* **81**, 3263 (1998).
- ¹⁶J. S. Im, H. Kollmer, J. Off, A. Sohmer, F. Scholz, and A. Hangleiter, *Phys. Rev. B* **57**, R9435 (1998).